Turkish Journal of Electrical Engineering & Computer Sciences

http://journals.tubitak.gov.tr/elektrik/

Research Article

Turk J Elec Eng & Comp Sci
(2016) 24: 558 – 570

doi:10.3906/elk-1309-206

Passivity-based robust controller design for a variable speed wind energy conversion system

Peng WANG[1,*], **Haisong WANG**[1], **Xu CAI**[1,2], **Zhengzhi HAN**[1]

[1]Wind Power Research Center, Department of Electrical Engineering, Shanghai Jiao Tong University, Shanghai, P.R. China

[2]State Key Laboratory of Ocean Engineering, School of Naval Architecture, Ocean, and Civil Engineering, Shanghai Jiao Tong University, Shanghai, P.R. China

Received: 26.09.2013 • **Accepted/Published Online:** 18.12.2013 • **Final Version:** 05.02.2016

Abstract: This paper proposes a design method for a robust controller to improve the stability and system dynamic behavior for variable speed wind energy conversion systems. By analyzing the mathematical model of a wind power conversion system, control strategies for both a generator-side converter and a grid-side converter are given. For the generator-side converter, the well-known maximum power point tracking method is employed, while for the grid-side converter, a robust controller is presented based on passivity theory. The L_2-gain performance is analyzed using linear matrix inequality. Moreover, in order to accelerate the dynamic response and reduce the DC link voltage fluctuations, the optimum equilibrium points of the system are designed based on the analysis of the dynamic equations of the DC link voltage. Finally, the proposed method is verified a by hardware-in-the-loop simulation.

Key words: Wind energy conversion system, robust controller, L_2-gain, linear matrix inequality, dynamic response

1. Introduction

Due to the advantages of the controllable power factor, bidirectional power flows, reduced current distortions, and high reliability, 2-level back-to-back PWM converters have been widely applied in the wind power industry [1–6]. In traditional applications, the DC link capacitors are used to decouple the generator-side converter and grid-side converter so that the 2 converters can be driven independently. However, the traditional method does not take the energy exchange on the DC link into consideration. If a high-value DC link capacitor is neglected, the DC link voltage cannot be maintained in a reasonable operation range under instantaneous load power variations. Moreover, a large capacitor not only increases the system cost but also raises the system failure rates. To reduce the DC link capacitor, there have been many methods presented to suppress the large voltage fluctuation [7–15]. In [7], Choi and Sul proposed an improved method to accelerate the transient response using dq-axis cross-coupling. In [8], Liutanakul et al. applied the decoupling system matrix to analyze the whole converter system. The authors of [9–12] proposed nonlinear feedforward power load compensation on the grid-side converter to improve the response speed. The authors of [13–15] used the exact I/O feedback linearization technique to decouple the converter system and realize the design of the system controller using a linear PI controller and nonlinear sliding mode controller. Nevertheless, it needs to be determined whether there are unstable zero-dynamics of the system using the exact I/O feedback linearization technique. Furthermore,

*Correspondence: w-fsfe@163.com

this technique could not completely decouple the 2 side converters because of the existence of uncertain model parameters.

For several decades, the passivity-based design has been a hot topic in the field of control theory. It has proven to be a powerful tool for nonlinear systems [16–18]. Recently, applications of passivity theory in the motor and converter control problem have been reported [19–24]. The authors of [19,20] used passivity theory to design an induction motor torque and speed controller. The authors of [21,22] applied the passivity theory to the control of a boost converter, and the authors of [23,24] analyzed the design principles of a passivity-based controller in a 3-phase PWM rectifier with a resistive load. In [24], the current control mode and voltage control mode were studied based on the Euler–Lagrange (EL) model. The cascade controller structure based on the PI regulator of the DC link voltage and the passivity-based current controller was also proposed. However, in these studies, the robustness of the current controller was not considered. Robust control is very important and useful, and so it is being rapidly developed nowadays [25–28]. If the control parameters are not appropriate, the current tracking performance is still affected by model uncertainties. One well-known technique for the robustness is L_2-gain control, which has been studied by many authors, for example in [26–28]. The authors of [26,27] used an adaptive L_2-gain controller for the power system, and Zhao and Hill [28] utilized L_2-gain analysis for a switched system. In these studies, the aim of the design was to reduce the magnitude of effect of the disturbance under the meaning of the L_2 norm.

Motivated by the above discussion, this paper studies the L_2-gain control problem and DC link voltage fluctuation suppression for a wind energy conversion system based on the passivity-based theory. The challenge of the paper mainly lies in two areas: the first is how to design the proper controller for wind energy conversion systems that contain uncertainties. The other is how to optimize the equilibriums by which the performance of the closed-loop system can be improved. Compared to other current studies, this paper presents a brand new approach. The contribution of the paper is that the passivity theory is first employed to analyze and design the stabilization and L_2-gain control problem for wind energy conversion systems. The linear matrix inequality (LMI) condition is derived to reduce the effects of parameter perturbation, and the optimization of the equilibriums is addressed to improve the response of the system for reducing the DC link capacitor in practice.

The remainder of the paper is organized as follows: Section 2 deals with the mathematical model. In Section 3, the controller is designed for a wind energy conversion system. Section 4 is devoted to the validation of the proposed method using hardware-in-the-loop (HIL) simulations. The last section is the conclusion.

2. Mathematical model of the wind energy conversion system

The topology of a full-scale power converter based on a squirrel cage induction generator (SCIG) is shown in Figure 1. This type of wind turbine consists of blades, a gear box, a SCIG, a back-to-back PWM converter, and a grid-connected line filter. Among them, the PWM converter plays a critical role; it is used to achieve the mode of variable speed constant frequency for the wind turbine. The converter consists of 2 parts: the generator-side converter and the grid-side converter. In this section, the mathematical models of each converter will be given.

2.1. Model of the generator-side converter

Under the rotary direct and quadrature (dq)-axis reference frame (by coordinate transformation based on an invariable norm), a 5-order mathematic model of the SCIG can be written as follows:

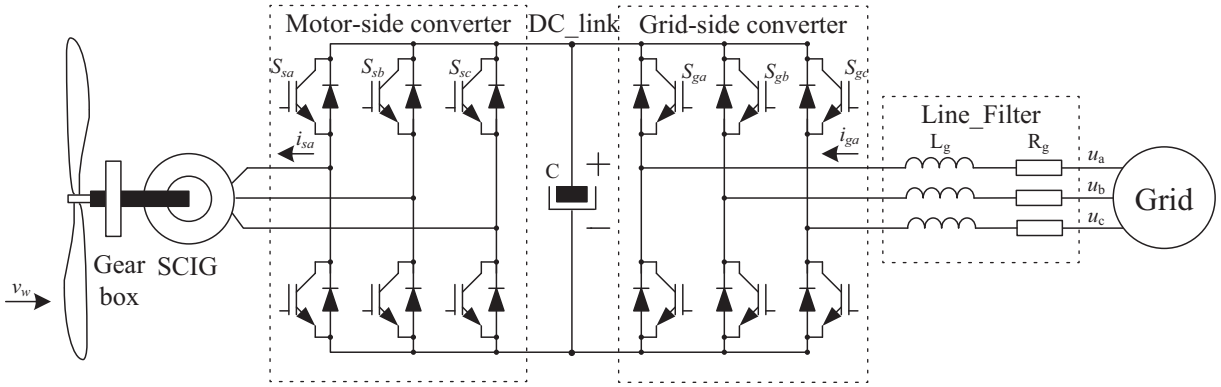

Figure 1. The topology of the full scale power converter based on a SCIG with turbines.

$$\frac{di_{sd}}{dt} = -\frac{R_s L_r^2 + R_r L_m^2}{\sigma L_s L_r^2} i_{sd} + \omega_1 i_{sq} + \frac{L_m}{\sigma L_s L_r T_r}\psi_{rd} + \frac{L_m}{\sigma L_s L_r}\omega_r \psi_{rq} + \frac{u_{sd}}{\sigma L_s}, \tag{1}$$

$$\frac{di_{sq}}{dt} = -\omega_1 i_{sd} - \frac{R_s L_r^2 + R_r L_m^2}{\sigma L_s L_r^2} i_{sq} + \frac{L_m}{\sigma L_s L_r T_r}\psi_{rq} - \frac{L_m}{\sigma L_s L_r}\omega_r \psi_{rd} + \frac{u_{sq}}{\sigma L_s}, \tag{2}$$

$$\frac{d\psi_{rd}}{dt} = \frac{L_m}{T_r} i_{sd} - \frac{1}{T_r}\psi_{rd} + (\omega_1 - \omega_r)\psi_{rq}, \tag{3}$$

$$\frac{d\psi_{rq}}{dt} = \frac{L_m}{T_r} i_{sq} - \frac{1}{T_r}\psi_{rq} - (\omega_1 - \omega_r)\psi_{rd}, \tag{4}$$

$$\frac{d\omega_r}{dt} = \frac{n_P}{J_m} T_e - \frac{n_p}{J_m} T_L, \tag{5}$$

where u_{sd}, u_{sq}, i_{sd}, and i_{sq} are stator voltages and currents in the dq-axis reference frame, respectively; R_s and R_r are the stator and rotor resistances, respectively; L_s, L_r, and L_m stand for stator inductance, rotor inductance, and mutual inductance, respectively; ψ_{rdq} is the rotor flux in the dq-axis reference frame; T_e and T_L are the electromagnetic torque and load torque of the SCIG, respectively; J_m is the moment of inertia of the SCIG; n_p is the generator pole pairs; ω_x and ω_r are the synchronous electrical angular velocity and rotor electrical angular velocity of the SCIG, respectively; T_r is the rotor time constant ($T_r = L_r \ / \ R_r$); and σ is the leakage coefficient ($\sigma = 1 - L_m^2 \ / \ (L_s L_r)$). These parameters can be obtained by parameter identification [29].

2.2. Model of the grid-side converter

Under the rotary dq-axis reference frame, the mathematical model of the grid-side converter is given as follows:

$$\begin{bmatrix} \frac{di_{gd}}{dt} \\ \frac{di_{gq}}{dt} \\ \frac{dV_{dc}}{dt} \end{bmatrix} = \begin{bmatrix} -\frac{R_g}{L_g} & \omega_g & -\frac{S_{gd}}{L_g} \\ -\omega_g & -\frac{R_g}{L_g} & -\frac{S_{gq}}{L_g} \\ \frac{3S_{gd}}{2C} & \frac{3S_{gq}}{2C} & -\frac{1}{CR_L} \end{bmatrix} \begin{bmatrix} i_{gd} \\ i_{gq} \\ V_{dc} \end{bmatrix} + \begin{bmatrix} \frac{u_d}{L_g} \\ \frac{u_q}{L_g} \\ 0 \end{bmatrix}, \tag{6}$$

where u_{dq} and i_{gdq} are grid voltages and currents in the dq-axis reference frame, respectively; V_{dc} is the DC link voltage; L_g and R_g stand for the inductance and equivalent resistance of the line filter, respectively; C is

the DC link capacitor; ω_g is the grid voltage synchronous rotating angular velocity; S_{gdq} are switching functions in the dq-axis reference frame; and R_L is the equivalent load resistance on the DC link.

Eq. (6) can be rewritten in EL model form [24]:

$$M_c\dot{x} + (J_c + R_c)x = F_c, \tag{7}$$

where

$$x = [\ i_{gd} \quad i_{gq} \quad V_{dc}\ ]^T, M_c = diag(L_g, L_g, \frac{2}{3}C), R_c = diag(R_g, R_g, \frac{2}{3R_L}),$$

$$F_c = [\ u_d \quad u_q \quad 0\ ]^T, J_c = \begin{bmatrix} 0 & -\omega_g L_g & S_{gd} \\ \omega_g L_g & 0 & S_{gq} \\ -S_{gd} & -S_{gq} & 0 \end{bmatrix}.$$

Obviously, M_c is a symmetric and positive-definite matrix. J_c is an antisymmetric matrix ($J_c = -J_c^T$) that represents the internal energies transfer of system. R_c is a symmetric and positive-semidefinite matrix that reflects the dissipative behaviors of the system. F_c represents the energy exchange between the internal and external energies.

3. Optimal controller design

Based on the analysis of the mathematical models of the converter systems for both sides, the control strategies for the generator-side converter and the grid-side converter are given in this section.

3.1. Control strategy of the generator-side converter

The control objectives of the generator-side converter are to realize maximum power point tracking (MPPT) and support the proper reactive current for SCIG operations. In this paper, the MPPT control is achieved by using a lookup table of the rotor velocity of a SCIG using real-time detection. According to the real-time value of the rotor velocity, the corresponding electromagnetic torque (T_e^*) that needs to be supported can be obtained. We can then calculate the given value of the torque current (i_{sq}^*) with the following equation:

$$i_{sq}^* = \frac{2L_r T_e^*}{3n_p L_m \psi_r}, \tag{8}$$

where ψ_r is the rotor flux estimation, which can be calculated from Eq. (3), i.e.

$$\psi_r = \frac{L_m i_{sd}}{1 + sT_r}, \tag{9}$$

where s is the differential operator.

The given value of excitation current (i_{sd}^*) can be obtained as follows:

$$i_{sd}^* = \frac{\psi_r^*}{L_m} = \frac{u_{sm}}{\omega_e L_m}, \tag{10}$$

where u_{sm} is the amplitude of the rated line voltage and ω_e is the rated frequency of the SCIG.

Based on the field-oriented vector control strategy, the torque current and excitation current are decoupled. Hence, we can use two independent current proportional plus integral (PI) regulators to realize the

currents' tracking. After that, the control voltages for the generator-side converter at work are given as follows:

$$u_{sd} = k_{p1}(i_{sd}^* - i_{sd}) + k_{i1}\int_0^t (i_{sd}^* - i_{sd})dt, \tag{11}$$

$$u_{sq} = k_{p1}(i_{sq}^* - i_{sq}) + k_{i1}\int_0^t (i_{sq}^* - i_{sq})dt, \tag{12}$$

where k_{p1} and k_{i1} are the control parameters of the current PI controllers that can be tuned by using the 'optimum symmetrical' [30].

According to the discussions above, the block diagram of the control scheme of the generator-side converter is shown in Figure 2.

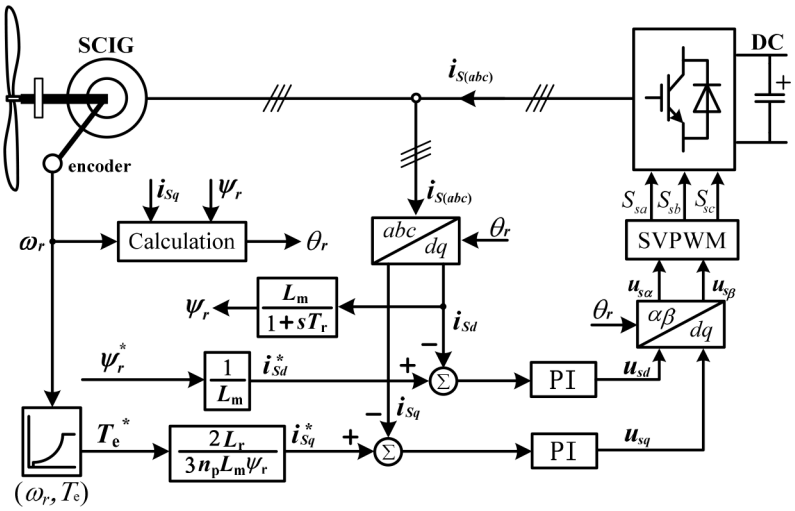

Figure 2. The block diagram of the control scheme of the generator-side converter.

In Figure 2, the angle θ_r of the rotor flux can be calculated as:

$$\theta_r = \int_0^t \omega_1 dt = \int_0^t (\omega_r + \omega_s)dt, \tag{13}$$

where ω_s is the slip frequency, which is defined as $\omega_s = \omega_1 - \omega_r$. We can obtain ω_s from Eq. (4) as follows:

$$\omega_s = \frac{L_m i_{sq}}{T_r \psi_r}. \tag{14}$$

3.2. The design of a robust controller for a grid-side converter

The control objectives of a grid-side converter are to maintain the DC link voltage at a constant value and ensure unit power factor operation. In this section, a robust controller based on the passivity theory is proposed. By using the cascaded controller structure [24], an outer DC link voltage PI controller is cascaded to an inner passivity-based current controller. For improving the robustness of the closed-loop control system, which has the properties of L_2 disturbance attenuation, the following control law will be used.

Considering that parameter uncertainties exist in the system, the, EL, model, from, Eq., (7), can, be, expressed, as:

$$(M_c + \Delta M_c)\dot{x} + (J_c + \Delta J_c)x + (R_c + \Delta R_c)x = F_c. \tag{15}$$

Using the bounded vector $w(x)$ instead of the disturbances, the system model can be transformed into the following expression:

$$M_c\dot{x} + J_c x + R_c x = F_c + w(x), \tag{16}$$

where $w(x) = \Delta M_c\dot{x} + \Delta J_c x + \Delta R_c x$.

Let $x_i^*, i = 1, 2, 3$ denote the desired equilibrium states of the closed-loop system. For the error state vector $e(e_i = x_i - x_i^*)$, the error dynamic equation is then expressed as:

$$M_c\dot{e} + J_c e + R_c e = F_c + w - M_c\dot{x}^* - J_c x^* - R_c x^*. \tag{17}$$

Let $z = Qe$, where Q is a nonsingular matrix. Then $\|z\|^2 = z^T z$ is used to evaluate the performance of errors.

Definition 1 *If there is a positive real number γ such that if $e(0) = 0$, and for all $T > 0$*

$$\int_0^T \|z\|^2 dt \le \gamma^2 \int_0^T \|w\|^2 dt \tag{18}$$

holds, then the system is L_2 disturbance attenuation with gain ω.

Remark 1 An alternative definition for the L_2 disturbance attenuation is as follows. If there is a positive definite function $V(e)$, which is continuous and differentiable, such that:

$$\dot{V}(e) \le \gamma^2 \|w\|^2 - \|z\|^2, \tag{19}$$

then taking the integration of Eq. (19) yields:

$$\int_0^T \|z\|^2 dt \le \gamma^2 \int_0^T \|w\|^2 dt + V(0). \tag{20}$$

Obviously, Eq. (20) is equivalent to Eq. (19). In the definition, we do not need the requirement of $e(0) = 0$. We will now give the main theorem of this paper.

Theorem 1 *Consider the system described by Eq. (17), if the controller is designed as*

$$F_c = M_c\dot{x}^* + J_c(x^* + e) + R_c x^* - R_a e, \tag{21}$$

where R_a satisfies

$$\begin{bmatrix} -R_a - R_c + \frac{1}{2}Q^T Q & \frac{1}{2}I \\ \frac{1}{2}I & -\frac{\gamma^2}{2}I \end{bmatrix} < 0, \tag{22}$$

then the system satisfies the following:

(a) When $w = 0$, the system is asymptotically stable at the expected equilibrium point.

(b) When $w \neq 0$, the system satisfies the L_2 gain condition in Eq. (20).

Proof For the system in Eq. (16), choosing the energy function $H = (1\ /\ 2)e^T M_c e$, we have:

$$\begin{array}{l} \dot{H} - \frac{1}{2}\gamma^2 \|w\|^2 + \frac{1}{2}\|z\|^2 \\ = e^T M_c \dot{e} - \frac{1}{2}\gamma^2 \|w\|^2 + \frac{1}{2}\|z\|^2 \\ = e^T (F_c + w - M_c \dot{x}^* - J_c(x^* + e) - R_c(x^* + e)) - \frac{1}{2}\gamma^2 \|w\|^2 + \frac{1}{2}\|z\|^2 \end{array} . \tag{23}$$

Substituting Eq. (21) into Eq. (23), we have:

$$\dot{H} - \frac{1}{2}\gamma^2 \|w\|^2 + \frac{1}{2}\|z\|^2 = \begin{bmatrix} e \\ w \end{bmatrix}^T \begin{bmatrix} -R_a - R_c + \frac{1}{2}Q^T Q & \frac{1}{2}I \\ \frac{1}{2}I & -\frac{\gamma^2}{2}I \end{bmatrix} \begin{bmatrix} e \\ w \end{bmatrix}. \tag{24}$$

In view of Eq. (22), the following holds:

$$\dot{H} \le \frac{1}{2}\gamma^2 \|w\|^2 - \frac{1}{2}\|z\|^2 . \tag{25}$$

Integrating Eq. (25) from 0 to infinity, we have:

$$H(\infty) - H(0) \le \frac{1}{2}\int_0^\infty \gamma^2 \|w\|^2 dt - \frac{1}{2}\int_0^\infty \|z\|^2 dt. \tag{26}$$

From the above results, we have the following conclusions:

(a) When $w = 0$, $H(\infty) - H(0) \le -\frac{1}{2}\int_0^\infty \|z\|^2 dt \le 0$ holds. It is concluded that the error system is asymptotically stable at the expected equilibrium points.

(b) When $w \ne 0$, considering $H \ge 0$, we have $\int_0^T \|z\|^2 dt \le \int_0^T \gamma^2 \|w\|^2 dt + H(0)$; that is, the L_2-gain is satisfied. Thus, we have completed the proof. □

For a grid-side converter, using grid voltage vector-oriented technology, we have $u_d = u_m$, $u_q = 0$. Hence, according to Eq. (21), the switching functions S_{gd} and S_{gq} can be obtained as follows:

$$S_{gd} = (u_d + \omega_g L_g i_{gq} - R_g i^*_{gd} + R_{a1}(i_{gd} - i^*_{gd}))/V_{dc}, \tag{27}$$

$$S_{gq} = (-\omega_g L_g i_{gd} + R_{a2}(i_{gq} - i^*_{gq}))/V_{dc}, \tag{28}$$

where R_{a1} and R_{a2} are diagonal elements of R_a.

To achieve the control objectives of the grid-side converter, the equilibrium points of the system states are set in the following forms:

$$i^*_{gq} = 0, \tag{29}$$

$$V^*_{dc} = V_{dc\_set}. \tag{30}$$

Then, assuming that the copper loss of the generator is negligible, substituting the control laws of Eqs. (27) and (28) into Eq. (6) yields:

$$\begin{array}{rcl} \dot{V}_{dc} & = & 3(u_d i^*_{gd} - R_g i^{*2}_{gd} + R_{a1}(i_{gd} - i^*_{gd})i^*_{gd} + R_{a2}(i_{gq} - i^*_{gq})i^*_{gq} - 2P^*_m/3)/(2V_{dc}C) \\ & = & 3(u_d i^*_{gd} - R_g i^{*2}_{gd} + R_{a1}(i_{gd} - i^*_{gd})i^*_{gd} + R_{a2}(i_{gq} - i^*_{gq})i^*_{gq} - (2/3)T^*_e \omega_r / n_p)/(2V_{dc}C). \end{array} \tag{31}$$

As tracking in the states is achieved, i.e. $i_{gd} \to i_{gd}^*$ and $i_{gq} \to i_{gq}^* = 0$, the equilibrium point of the d-axis current of the grid-side converter can be calculated as follows:

$$i_{gd}^* = (R_g i_{gd}^{*2} + (2/3)T_e^* \omega_r / n_p)/u_d. \tag{32}$$

In Eq. (32), due to $R_g i_{gd}^{*2} \ll (2/3)T_e^* \omega_r / n_p$, we get:

$$i_{gd}^* = (2/3)T_e^* \omega_r / (n_p u_d). \tag{33}$$

To accelerate the dynamic response speed of the grid-side converter, we add the result of Eq. (33) to the output of the DC link voltage PI controller as feedforward compensation. Afterwards, the dynamic equilibrium point of the d-axis current can be designed as:

$$i_{gd}^* = k_{p2}(V_{dc}^* - V_{dc}) + k_{i2} \int_0^t (V_{dc}^* - V_{dc})dt + \frac{2T_e^* \omega_r}{3u_d n_p}, \tag{34}$$

where k_{p2} and k_{i2} are the control parameters of the DC link voltage PI controllers.

In conclusion, the block diagram of the robust control scheme of the grid-side converter is given in Figure 3.

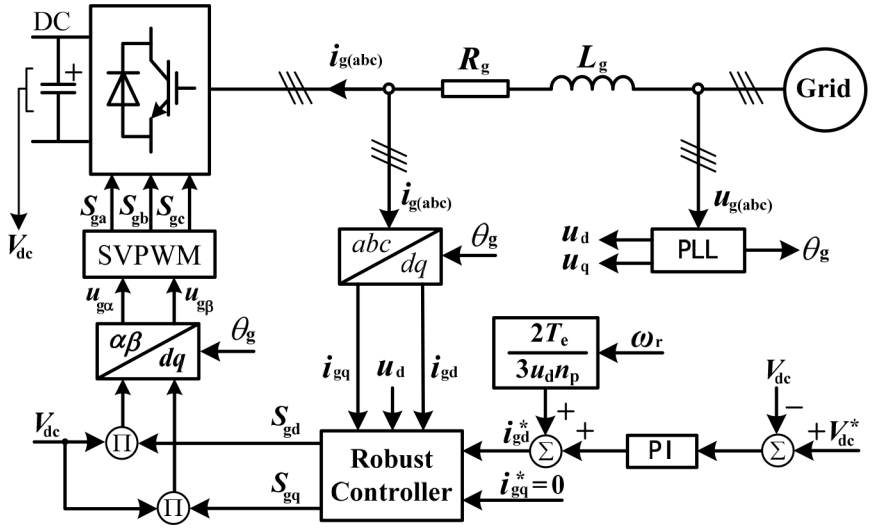

Figure 3. The block diagram of the robust control scheme of the grid-side converter.

4. System performance verification using HIL simulation

In this paper, the proposed control method is verified using RT-LAB, which is an integrated real-time simulation platform for rapid and automatic implementation in real-time on a standard PC platform, used for rapid control prototyping and HIL simulation [31,32]. RT-LAB uses Simulink as a front end for editing and viewing graphic models. Hence, we use it to simulate the hardware configuration of a 2.5 MW full-scale power converter based on the SCIG. The system parameters of HIL simulation are given in the Table, and the control algorithms are realized using a digital controller based on the TMS320F6747 DSP. The HIL simulation results contain 2 parts: the assessment of the dynamic response characteristics of the proposed control method in comparison to the traditional PI controller, and the system performance under model uncertainties.

Table. Parameters of HIL simulation.

Quantity	Value
Rated power p_e/kW	2500
Rated line voltage U_e/V	690
Rated frequency f_G/Hz	50
Filter inductance L_g / μH	132
Equivalent resistance of line filterR_g / mΩ	2
DC link capacitor C/mF	59.4
Rated voltage of DC link V_{dc}^* / V	1100
Stator self-inductance of generator $L_s^{'}$ / mH	0.03694
Stator resistance of generator R_s / mΩ	0.8487
Rotor self-inductance of generator $L_r^{'}$ / mH	0.03331
Rotor resistance of generator R_r / mΩ	0.6928
Mutual inductance of generator L_m / mH	1.187
Moment of inertia of generator J/ (kg m^2)	2400
Pole pairs of generator n_p	3
Rated torque of generator T_e / N m	24670
Converter switching frequency f_s / kHz	3
Calculation time in HIL simulations t_{HIL} / μs	20

4.1. Dynamic response characteristics

The dynamic response characteristics are investigated under varying load conditions (no-load to full-load) with a rated speed of 104.7 rad/s. For stabilizing the speed of the SCIG, an outer speed PI controller is added into the generator control. Before 2 s, the wind energy conversion system works in no-load operation. At 2 s, the load variation happens, and the system dynamic performance is shown in Figures 4–7.

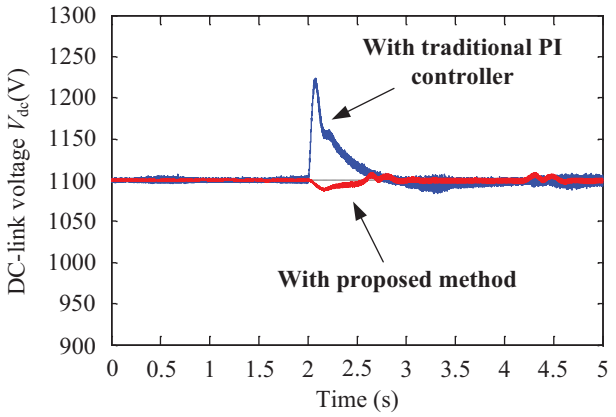

Figure 4. The fluctuation of the DC link voltage under load variation.

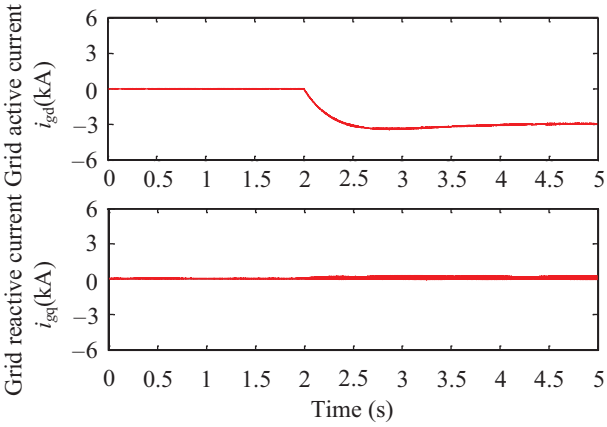

Figure 5. Dynamic responses of grid currents.

Figure 4 shows the dynamic responses of the DC link voltage with both the proposed passivity-based controller and the traditional PI controller. It can be observed that when the traditional PI controller is applied, a large voltage fluctuation appears on the DC link. The maximum value of the DC link voltage is up to 1220 V. On the contrary, the DC link voltage is insensitive to load variation using the method proposed in this paper. This is because the response speed is restricted by the integrator of the PI controller of the DC link voltage in

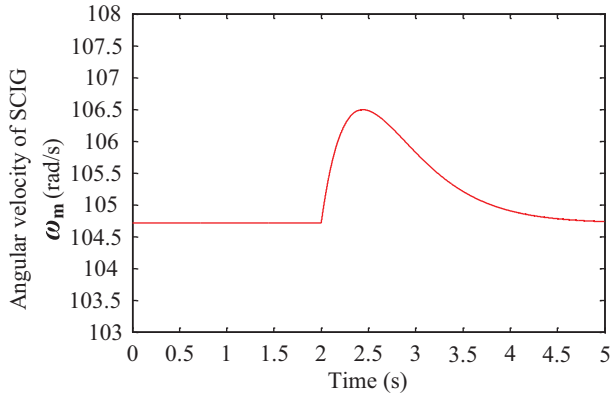

Figure 6. Dynamic response of the rotor angular velocity of the SCIG.

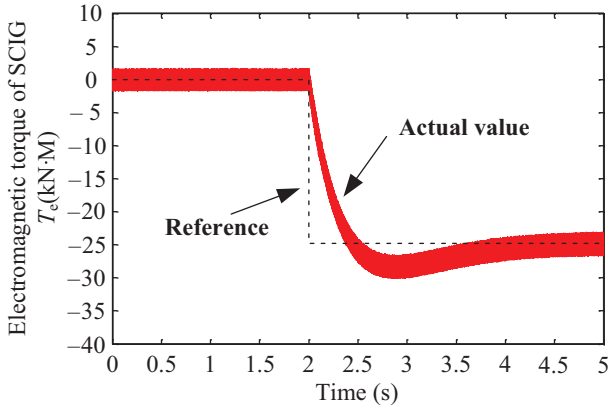

Figure 7. Dynamic response of the electromagnetic torque of the SCIG.

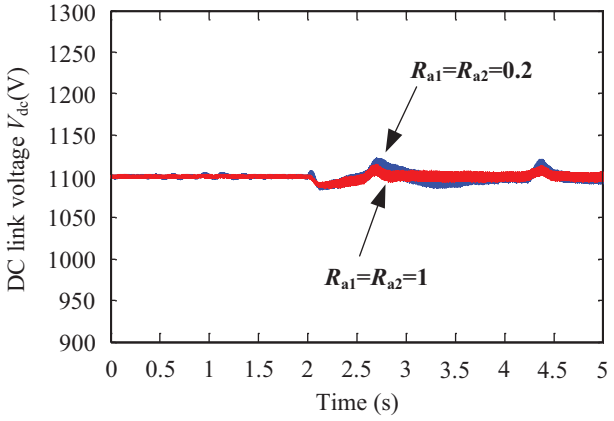

Figure 8. Dynamic response of the DC link voltage with uncertain parameters: (a) active current i_{gd}, (b) reactive current i_{gq}.

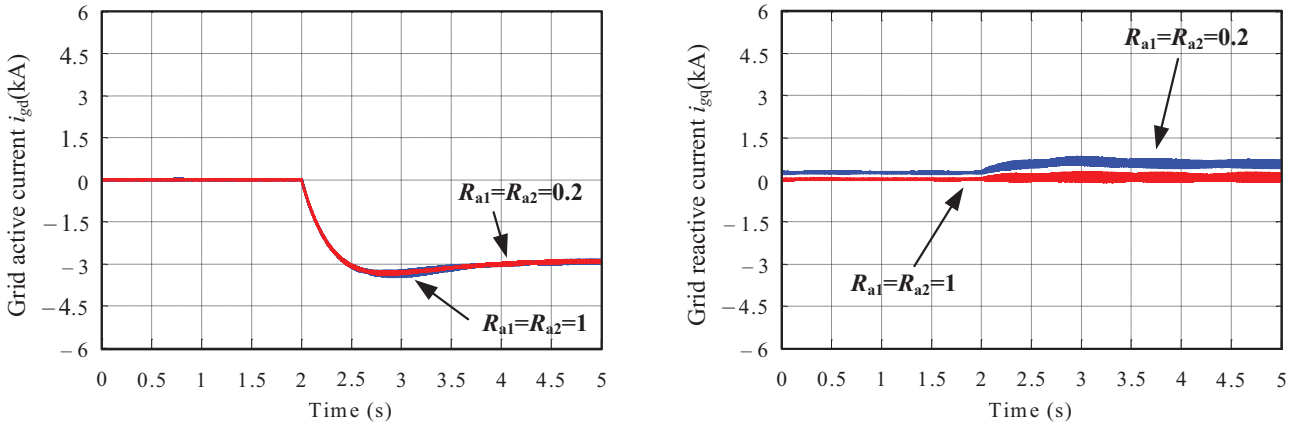

(a)active current i_{gd} (b)reactive current i_{gq}

Figure 9. Dynamic responses of grid currents with uncertain parameters.

the traditional method while the effectiveness of the integrator is removed by optimizing the equilibrium points of the control system. Hence, the response speed is improved under load variation.

Figure 5 shows the dq-axis currents of the grid-side converter. We can see that both the active current i_{gd} and the reactive current i_{gq} behave with good dynamics and steady characteristics. Moreover, the reactive current i_{gq} fluctuates around 0. The unity power factor operation is then achieved.

The dynamic response of the rotor angular velocity and the electromagnetic torque of the SCIG are shown in Figures 6 and 7, respectively. It is obvious that the rotor angular velocity of the SCIG increases due to the sudden change of input torque from no-load to full-load. The electromagnetic torque can track the input load torque within about 2.5 s.

The HIL simulation results show that the proposed robust control method has good performance under load variations and steady state operations.

4.2. Robust performance of the system with parameter variation

In this section, the robust performance of the control system is checked. In the HIL simulation, the filter inductance of the grid-side converter is set to 100% larger than the value given in the Table. The equivalent resistance of the line filter is set to 100% larger than that used in controller design. In the meantime, the DC link capacitance is set to half of that used before. According to the solution of LMI in Eq. (22), the control system could have the properties of L_2 disturbance attenuation by selecting $R_{a1} > 0.496$ and $R_{a2} > 0.496$. To verify the validity of the proposed robust controller, we use $R_{a1} = R_{a2} = 0.2$ and $R_{a1} = R_{a2} = 1$ in the HIL simulations. With the same setup of working environments as in the last section, the simulation results are shown in Figures 8 and 9.

The dynamic characteristics of the DC link voltage under load variation are shown in Figure 8, and the dq-axis actual currents of the grid-side converter are given in Figure 9. It is observed that the DC link voltage can also be maintained at the given value with a different setting of R_a, and the active currents are generally the same. However, the reactive currents are different with a different control law. It can be seen that the reactive current i_{gq} could not converge to 0 with parameter variation. Hence, the power factor is reduced. It should be noted that the power factor can be corrected if the controller satisfies the L_2-gain conditions. Meanwhile, it is implied that the active current is not influenced by parameter uncertainty because of the use of the outer DC link voltage PI loop. This conclusion is similar to the results in [24]. To sum up, by properly designing the control parameters, the control performance of a system with uncertain parameters can be guaranteed. Additionally, the DC link capacitor can also be reduced by the proposed method.

5. Conclusions

By analyzing the mathematical model of a full-scale power converter based on the SCIG, a passivity-based robust controller for a wind energy conversion system is first designed. Under the designed control law, the stability of the error system can be guaranteed, and the L_2 disturbance attenuation can also be obtained according to the LMI constraints. In view of these results, the optimum equilibrium points of the system states are designed in order to improve the dynamic performance of the control system. Finally, the proposed control method is verified by HIL simulations.

Acknowledgments

This work was supported by the National High Technology Research and Development Program of China (003 2011AA05A104) and the Shanghai Science Foundation project (11dz1200204).

References

[1] Ooi TJ, Dixon BW, Kulkarni AB, Nishimoto M. An integrated AC drive system using a controlled-current PWM rectifier/inverter link. IEEE T Power Electr 1988; 3: 64–71.

[2] Tang Y, Xu L. A flexible active and reactive power control strategy for a variable speed constant frequency generating system. IEEE T Power Electr 1995; 10: 472–478.

[3] Malekian K, Shirvani A, Schmidt U, Schufft W. Detailed modeling of wind power plants incorporating variable-speed synchronous generator. In: Electrical Power & Energy Conference, 22–23 October 2009; Montreal, Canada. New York, NY, USA: IEEE. pp 1–6.

[4] Dai JC, Hu YP, Liu DS, Wei J. Modelling and analysis of direct-driven permanent magnet synchronous generator wind turbine based on wind-rotor neural network model. J Power Energ 2012; 226: 62–72.

[5] Wu F, Zhang XP, Ju P, Sterling MJH. Optimal control for AWS-based wave energy conversion system. IEEE T Power Syst 2009: 24: 1747–1755.

[6] Simões MG, Bose BK, Spiegel RJ. Fuzzy logic-based intelligent control of a variable speed cage machine wind generation system. IEEE T Power Electr 1997; 12: 87–95.

[7] Choi JW, Sul SK. Fast current controller in three-phase AC/DC boost converter using d-q axis crosscoupling. IEEE T Power Electr 1998; 13: 179–185.

[8] Liutanakul P, Pierfederici S, Meibody-Tabar F. DC-link capacitor reduction of a controlled rectifier supplying N inverter-motor drive systems by compensating the load variations. In: IEEE 35th Annual Power Electronics Specialists Conference; 1 January 2004; Aachen, Germany. New York, NY, USA: IEEE. pp. 1298–1303.

[9] Malesani L, Rossetto L, Tenti P, Tomasin P. AC/DC/AC PWM converter with reduced energy storage in the DC link. IEEE T Ind Appl 1995; 31: 287–292.

[10] Hur N, Jung J, Nam K. A fast dynamic DC-link power-balancing scheme for a PWM converter-inverter system. IEEE T Ind Appl 2001; 48: 794–803.

[11] Gu BG, Nam K. A DC-link capacitor minimization method through direct capacitor current control. IEEE T Ind Appl 2006; 42: 573–581.

[12] Nejad MAS, Pierfederici S, Martin JP, Meibody-Tabar F. Study of an hybrid current controller suitable for DC-DC or DC-AC applications. IEEE T Power Electr 2007; 22: 2176–2186.

[13] Jung J, Lim S, Nam K. A feedback linearizing control scheme for a PWM converter-inverter having a very small DC-link capacitor. IEEE T Ind Appl 1999; 35: 1124–1131.

[14] Lee DC, Lee GM, Lee KD. DC-bus voltage control of three-phase AC/DC PWM converters using feedback linearization. IEEE T Ind Appl 2000; 36: 826–833.

[15] Liutanakul P, Pierfederici S, Meibody-Tabar F. Application of SMC with I/O feedback linearization to the control of the cascade controlled-rectifier/inverter- motor drive system with small DC-link capacitor. IEEE T 2008; 23: 2489–2499.

[16] Isidori A. Nonlinear Control Systems. New York, NY, USA: Springer-Verlag, 1999.

[17] Ortega R, Loria A, Nicklasson PJ, Sira-Ramirez HJ. Passivity-Based Control of Euler-Lagrange Systems. New York, NY, USA: Springer-Verlag, 1998.

[18] Ortega R, Loria A, Nicklasson PJ, Sira-Ramirez HJ. Passivity-Based Control of Euler-Lagrange Systems: Mechanical, Electrical and Electromechanical Applications. London, UK: Springer-Verlag, 1998.

[19] Gonzalez H, Duarte-Mermoud MA, Pelissier I, Travieso-torres JC, Ortega R. A novel induction motor control scheme using IDA-PBC. J Control Theor Appl 2008; 6: 59–68.

[20] Cecati C, Rotondale N. Torque and speed regulation of induction motors using the passivity theory approach. IEEE T Ind Electr 1999; 46: 119–127.

[21] Leyva R, Cid-Pastor A, Alonso C, Queinnec I, Tarbouriech S, Martinez-Salamero L. Passivity-based integral control of a boost converter for large-signal stability. IET Control Theor Appl 2006; 153: 139–146.

[22] Linares-Flores J, Reger J, Sira-Ramírez H. Load torque estimation and passivity-based control of a boost-converter/DC-motor combination. IEEE T Syst Control Tech 2010; 18: 1398–1405.

[23] Leyva R, Olalla C, Queinnec I, Tamura K. Passivity-based control for large-signal stability of high-order switching converters. Asian J Control 2012; 14: 335–347.

[24] Lee TS. Lagrangian modeling and passivity-based control of three-phase AC/DC voltage-source converters. IEEE T Ind Electr 2004; 51: 892–902.

[25] Burkan R. Design of adaptive compensators for the control of robot manipulators robust to unknown structured and unstructured parameters. Turk J Electr Eng Co 2013; 21: 452–469.

[26] Shen T, Ortega R, Lu Q, Mei SW. Adaptive L_2 disturbance attenuation of Hamiltonian systems with parametric perturbation and application to power systems. Asian J Control 2003; 5: 143–152.

[27] Wang Y, Cheng D, Li C, Ge Y. Dissipative Hamiltonian realization and energy-based L_2-disturbance attenuation control of multimachine power systems. IEEE T Autom Control 2003; 48: 1428–1433.

[28] Zhao J, Hill DJ. On stability, L_2-gain and H_∞ control for switched systems. Automatica 2008; 44: 1220–1232.

[29] Benaidja N. Softcomputing identification techniques of asynchronous machine parameters: evolutionary strategy and chemotaxis algorithm. Turk J Electr Eng Co 2009; 17: 69–85.

[30] Leonhard W. Control of Electrical Drives. New York, NY, USA: Springer-Verlag, 2001.

[31] Abourida S, Dufour C, Bélanger J, Yamada T, Arasawa T. Hardware-in-the-loop simulation of finite-element based motor drives with RT-Lab and JMAG. In: IEEE International Symposium on Industrial Electronics; 9–13 July 2006; Montreal, Canada. New York, NY, USA: IEEE. pp 2462–2466.

[32] Ivanovic Z R, Adzic E M, Vekic M S, et al. HIL evaluation of power flow control strategies for energy storage connected to smart grid under unbalanced conditions. IEEE T Power Electr 2012; 27: 4699–4710.